Quantitative evaluation of the response to neo-adjuvant chemotherapy based on non-rigid registration of CEM

Clément Jailin, Pablo Milioni de Carvalho, Sara Mohamed, Laurence Vancamberg, Amr Farouk Ibrahim Moustafa, Mohammed Mohammed Gomaa, Rasha Mohammed Kamal, Serge Muller

QUANTITATIVE EVALUATION OF THE RESPONSE TO NEO-ADJUVANT CHEMOTHERAPY BASED ON NON-RIGID REGISTRATION OF CEM

Clément Jailin[†], *Pablo Milioni De Carvalho*[†], *Sara Mohamed*[†], *Laurence Vancamberg*[†], *Amr Farouk Ibrahim Moustafa*[⋆], *Mohammed Mohammed Gomaa*[⋆], *Rasha Mohammed Kamal*[⋆], *Serge Muller*[†]

[†] GE HealthCare, Buc, France
[⋆] Baheya Foundation For Early Detection And Treatment Of Breast Cancer, El Haram, Giza, Egypt

ABSTRACT

This paper introduces a new intensity-compensated longitudinal non-rigid registration method for Contrast Enhanced Mammography monitoring neoadjuvant chemotherapy (NAC). The registered NAC image subtraction, called residual fields, allows to discriminate between different lesion responses to treatment using features extraction. The approach registers low-energy 2D images of the exams acquired before and after the chemotherapy. The measured motion is then applied to the corresponding dual-energy recombined images. Consequently, the difference in registered images allows identifying local density and iodine uptake changes, especially in the lesion area. The registration converged for all 51 patients with 208 image pairs. Finally, the residual fields can be used to extract clinically relevant features used to assess the response of the treatment. The lesion response classification model, evaluated with the AUC and F-score, performed better when taking into account the residual features (AUC: 0.92 vs 0.79).

***Index Terms*—** Breast imaging, Neoadjuvant Chemotherapy, Contrast Enhanced Mammography, Registration

1. INTRODUCTION

Neoadjuvant chemotherapy (NAC) is a therapeutic option increasingly used in the management strategy for breast cancer. The main goal of NAC is the reduction of tumor volume and metastasis leading to an increase in breast-conserving surgery probabilities instead of mastectomy. NAC also allows early assessment of the efficiency of systemic therapy in-vivo which could lead to a revision of the treatment plan in cases that show poor response. The extent of residual invasive cancer after neoadjuvant therapy is also a prognostic factor for the risk of recurrence. Imaging the breast before, sometimes during, and after the NAC is important to evaluate the treatment response and future treatment planning. A precise assessement and quantification of the tumor response is a precious information shared during the multi-disciplinary tumor board, between the radiologist, the surgeon and the oncologist.

Contrast-Enhanced Magnetic Resonance Imaging (CE-MRI) is the imaging modality generally used to monitor response to NAC. Various studies have developed 3D deformable CE-MRI registration procedures to extract quantitative features in pre-NAC and/or post-NAC images related to lesion evolution [1, 2].

Contrast-Enhanced Mammography (CEM) provides anatomical and functional imaging of breast tissue improving the accuracy of breast cancer diagnosis [3]. As an alternative to CE-MRI, the competence of CEM in the assessment and prediction of response to NAC has been studied [4, 5] using image lesion measurements. In addition, some studies presented a method extracting quantitative features to evaluate residual disease extents [6, 7, 8]. These approaches are based on intensity features (*e.g.,* radiomics) extracted from the low-energy and recombined images.

Because the breast cannot be similarly re-positioned between two exams, registration in 2D mammography has been studied for an easier breast texture comparison. Many registration approaches have been developed such as feature-based [9], intensity-based [10] and deep-learning-based [11] methods. The major challenges for these state-of-the-art breast registration approaches are large displacements and important intensity variations. Those issues are exacerbated when dealing with NAC cases composed of large tumors that may shrink or disappear (for complete pathological responses).

The goal of this paper is to present a lesion response classification based on registered NAC-CEM images. The proposed non-rigid registration procedure handles large repositioning displacements, important intensity changes at a high convergence rate. The residual fields obtained after registration are then used to extract intensity evolution features for the lesion response classification. The first section presents the NAC-CEM database. Then, the state of the art and proposed registration method (GDIC-I), enhanced with local intensity corrections, is presented as well as the lesion response classification method. Finally, an evaluation of the registration and classification is performed.

2. MATERIALS

In CEM-NAC monitoring, the patient is imaged with a CEM acquisition pre-NAC and post-NAC. The CEM acquisition consists of a low-energy (LE) image and a high-energy (HE) image processed into a so-called recombined (REC) image that highlights the iodine content. After the acquisition, the extent of the disease are reported in pre-NAC and post-NAC studies. Radiological response to NAC is assessed once applying the Response Evaluation Criteria in Solid Tumor [10]: RECIST 1.1. This evaluation is using the ratio of the longest length of the lesion before and after NAC. After the treatment, the analysis of the surgical piece allows for identifying the completeness of the pathological response.

In our study, fifty-one patients with pathologically proven breast cancer based on the tumor tissues obtained by core needle biopsy were enrolled. All data were acquired at *Baheya Foundation For Early Detection And Treatment Of Breast Cancer, Giza, Egypt*. Patients were all planned to receive NAC in reference to the breast cancer tumor board decision. As both breasts were imaged with multiple views (at least CC and MLO views for the two breasts), 107 acquired

image pairs of the malignant breast were acquired and 101 pairs of the non-affected contralateral breasts. Examinations were performed with a Senographe Pristina™ (*GE HealthCare, Chicago, IL, USA*). The study protocol was approved by the Institutional Review Board and informed written consent was applied using the data use of the enrolled individuals. All 52 biopsied lesions were invasive ductal carcinoma. Finally, after surgery, 14 cases were pathology-proven complete responses, 39 partial responses (more than 30% decrease), 6 insensitive responses (3 stable diseases (up to 20% increase), and 3 progressive diseases).

Patients with metastatic disease, pregnant females, and those who gave a history of allergy to contrast media, or renal impairment were omitted from the study.

The image annotations were performed by senior radiologists specialized in breast imaging. One NAC-CEM case is presented in Fig. 1. The green boxes in the pre-NAC and post-NAC acquisitions are the radiologist cancer annotations.

3. METHOD

3.1. Optical flow registration

Given a pair of images, an initial pre-NAC image $f(\boldsymbol{x})$ and a target post-NAC acquisition $g(\boldsymbol{x})$, the intensity-based methods define a spatial residual $\rho_u(\boldsymbol{x})$ that can be written, with $\boldsymbol{u}(\boldsymbol{x})$ the Lagrangian displacement field: $\rho_u(\boldsymbol{x}, f, g, \boldsymbol{u}) = g(\boldsymbol{x}) - f(\boldsymbol{x} + \boldsymbol{u}(\boldsymbol{x}))$. The sought displacement correction field is the one that minimizes, on the data fidelity term over a spatial region of interest (ROI), a norm of the residuals ρ_u.

Different approaches have been developed in the literature to solve this problem. Two approaches will be evaluated as references: TV-L1 and GDIC. The popular TV-L1 approach [12] consists of an L1 data penalty term and total variation regularization with λ the penalization coefficient.

In global Digital Image Correlation (GDIC), the displacement is written as a finite element mesh kinematics composed of N_u nodes and shape functions $\{\phi\}$ for the interpolation [13]. The nodes (chosen by the nodal surface density) are positioned in the region of interest in the image such that the full breast surface is covered by the mesh. The triangular element generation is obtained with a Delaunay triangulation. The motion can thus be written, with a reduced set of nodal displacements u_l

$$\boldsymbol{u}(\boldsymbol{x}) = \sum_{l=1}^{N_u} u_l \boldsymbol{\phi}_l(\boldsymbol{x}). \tag{1}$$

Because registered breast images are acquired at different time intervals and treatment stages, the brightness conservation assumption is not respected due to factors extrinsic to the displacement (*e.g.,* evolution in the breast tissue, changes in the acquisition system).

3.2. Relaxed intensity conservation - GDIC-I

To consider large local intensity changes in the lesion area, an intensity compensation procedure, GDIC-I, is developed. The approach is based on a local brightness and contrast correction studied for material science [14]. The relaxed brightness conservation assumption redefines a correction model for the images by compensating the intensity variations with a spatial field $v(\boldsymbol{x})$: $\tilde{f}(\boldsymbol{x}) = v(\boldsymbol{x}, f(\boldsymbol{x}+\boldsymbol{u}(\boldsymbol{x})))$, where the latter can be written with a polynomial correction

$$v(\boldsymbol{x}, h(\boldsymbol{x})) = \sum_p v_p(\boldsymbol{x}) h^p(\boldsymbol{x}). \tag{2}$$

In this study, the correction is limited to the first two terms. The intensity corrected residual, written ρ_{uv} reads

$$\rho_{uv}(\boldsymbol{x}, f, g, \boldsymbol{u}, \boldsymbol{v}) = g(\boldsymbol{x}) - (v_0(\boldsymbol{x}) + v_1(\boldsymbol{x}) f(\boldsymbol{x} + \boldsymbol{u}(\boldsymbol{x}))) . \tag{3}$$

Similarly to the kinematic model, the intensity correction can also be regularized and written in a finite element framework

$$v_p(\boldsymbol{x}) = \sum_{l=1}^{N_v} v_{pl} \psi_l(\boldsymbol{x}), \tag{4}$$

with v_{pl} the N_v nodal intensity values and $\{\psi\}$ the intensity interpolation functions. The intensity mesh is generated using the same approach as the kinematic regularization.

Finally, a Gauss-Newton scheme is used to solve this nonlinear problem considering to the nodal motion and intensity amplitudes. To avoid possible poor conditioning, a penalization based on the comparison between the estimated displacement field and that of the solution to a homogeneous elastic problem [15, 16] is introduced. The penalization term is written in the finite element framework. The equilibrium equation, in the absence of nodal forces reads $\boldsymbol{K}\{u\} = \boldsymbol{0}$, with $\boldsymbol{K}$ the stiffness matrix and $\{u\}$ the set of nodal degrees of freedom. This additional term in the functional penalizes locally the motion that introduces strong elastic energy.

The kinematic and intensity meshes were generated from the control of the nodal surface density (kinematic mesh density was set to 1 node / 5 cm^2 and the intensity mesh distance was set to 1 node / 2 cm^2). Both kinematics and intensity finite element shape functions, $\{\phi\}$ and $\{\psi\}$, were chosen as bi-linear. The TV-L1 approach was applied with a generic hyper-parameter value [12]: $\lambda = 15$.

At convergence, the registered image difference can be computed as $\rho_{uv}(\boldsymbol{x}, f, g, \boldsymbol{u}, \boldsymbol{v} = \boldsymbol{0})$. This non-intensity compensated difference highlights the intensity changes. After registration, theses differences are assumed to correspond to density and iodine changes for respectively the low-energy and recombined residuals.

Transformation of CEM images. The recombined image essentially highlights the hypervascularized lesion area (that takes contrast). This area is subject to important intensity changes with the chemotherapy treatment. It is hence difficult to register a pair of recombined images. It is here proposed to register LE images that share most of their fibro-glandular and adipose texture. After the registration of LE images, REC pre-NAC image, written f_{Rec}, can be transformed using the measured displacement field: $f_{\text{Rec}}(\boldsymbol{x}+\boldsymbol{u}(\boldsymbol{x}))$. The recombined residual field hence defined with the post-NAC REC image g_{Rec} such as $\rho_{Rec}(\boldsymbol{x}, f_{\text{Rec}}, g_{\text{Rec}}, \boldsymbol{u}) = g_{\text{Rec}}(\boldsymbol{x}) - f_{\text{Rec}}(\boldsymbol{x} + \boldsymbol{u}(\boldsymbol{x}))$.

Registration evaluation 618 landmarks, written respectively $\boldsymbol{x}_f$ and $\boldsymbol{x}_g$ have been placed in respectively f and g on clearly identified textures (*e.g.,* calcification, nipple, infra-mammary fold, the center of nodules) in the LE and/or the REC image. The registered landmark distance $d = \|\boldsymbol{x}_g - \boldsymbol{x}_f - \boldsymbol{u}(\boldsymbol{x}_f)\|_2$ will be evaluated with the Root Mean Square Error (RMSE[d]) and maximal error (max[d]) as a metric of the registration quality.

3.3. Quantification of the lesion response

The goal of this session is to build a classification modeling the pathology response using image features extracted from the LE images, the REC image, and the residual fields. The output of this classifier consists of 3 classes: complete pathological response, partial response, and insensitive response (containing stable or progressive disease).

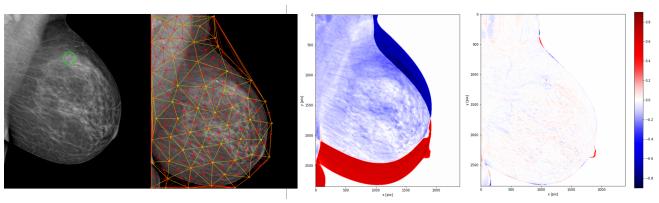

Fig. 1. Registration of a low-energy image pair. From left to right, the pre-NAC and post-NAC acquisitions, the uncorrected and corrected differences.

Because of a small accessible dataset and to avoid over-fitting, very few image features are chosen to be extracted on the ROI defined by the radiologist annotation: mean, standard deviation, L2 norm, 10^{th} and 90^{th} quantiles. Those features belong to the 1^{st} order radiomics. The ROI correspond to rectangles annotated in the images by experienced radiologist in breast and CEM imaging. The annotations are circumscribed to the lesion extents. It can be noted that this ROI selection could be performed automatically by a detection CEM-CAD [17].

Similarly to AI-based NAC assessment [8], the features extraction can be performed on the LE image and REC image for both the pre-NAC and post-NAC acquisitions. A total of 20 features are hence extracted.

The registered residual fields on the low-energy and recombined images can also be used. The 5 selected features are also extracted resulting in 10 additional features. It can be noted that the annotation in the residual images is defined by the union of the post-NAC annotation and the warped pre-NAC annotation. This union will be larger than the warped pre-NAC annotation essentially in progressive responses. After the normalization of the feature values, the classification model used was a linear discriminant analysis (LDA). This model allows performing simple linear classification with small datasets.

The features extraction was performed on the 107 lesions, considering each view independently. Because of the limited size of our dataset, the data were split into a training and a test set using the leave-one-out (patient-wise) cross-validation strategy. After the 51 trainings, the multi-label classification model was evaluated using the AUC of all individual classes (AUC of each class against the others [18]), the macro-average AUC, and the F-score.

4. RESULTS

Figure 1 shows the low energy registration results for one mediolateral oblique view with, from left to right, the pre-NAC and post-NAC acquisitions, the uncorrected and corrected differences. The two meshes (red for the kinematics, yellow for the intensity) are plotted on the post-NAC image. The large blue and red pattern that can be seen on the uncorrected residual are the signature of an uncorrected image alignment. This large pattern disappears in the corrected one highlighting a correct registration.

Figure 2 presents the complete registration results for one left mediolateral oblique view showing a partial pathological response. In this figure, the first line corresponds to LE images, and the second to REC images. (a-d), (b-e) and (c-f) are respectively the pre-NAC, post-NAC, and residual fields. The residual fields are shown with a divergent colormap to identify positive (in red) and negative (in blue) values. The lesion area annotated by the radiologist is highlighted with the green box. The registered residual fields in Figure 2

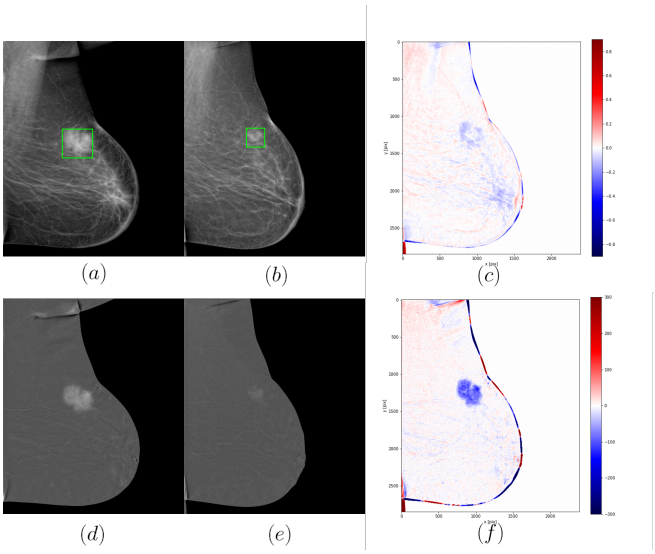

Fig. 2. Case of a partial radiological response. Top: LE, bottom: REC images with (a-d) the pre-NAC, (b-e) the post-NAC, (c-f) $\rho_{uv}(\boldsymbol{x}, f, g, \boldsymbol{u}, \mathbf{0})$ and $\rho_{Rec}(\boldsymbol{x}, f_{\text{Rec}}, g_{\text{Rec}}, \boldsymbol{u})$

	RMSE [mm]	Max distance [mm]
Initial	19.0	60.6
TV-L1	11.2	55.1
GDIC	8.1	32.2
GDIC-I	5.9	21.3

Table 1. Registration metrics on the landmarks positioning with different approaches.

show a map of intensity evolution (texture or iodine). A blue annulus in Figure 2(c) shows the concentric lesion shrinkage with the treatment. A density decrease can also be observed in the retro-areolar area. The dark blue area in Figure 2(f) is a projected iodine decrease on the lesion.

The evaluation of the registration method was computed on converged cases only (respectively 121/208,183/208, and 208/208 image pairs for the TV-L1, GDIC, and GDIC-I methods). The metrics are presented in the Table 1. The RMSE on the landmark repositioning was computed using TV-L1, GDIC, and GDIC-I and led to respectively 11.2 mm, 8.1 mm, and 5.9 mm while initially (without registration) at 19.0 mm. The maximal distance with the same models was respectively, for TV-L1, GDIC, and GDIC-I: 55.1 mm, 32.2 mm, and 21.3 mm (initially at 60.6 mm).

Figure 3 shows the lesion features projected onto the first axis of the LDA without (top) and with (bottom) using the features extracted from the residual fields. 107 markers are plotted for each apparition of a treated lesion. The colors and marker choice are the 3 classes of NAC response: complete pathological response - partial - insensitive. The obtained evaluation metrics for the LE and REC extraction are: AUC of 0.79 and the F1 score 0.58. With the use of residual features the AUC is 0.92 and F1 score 0.79.

Figure 4 displays the receiver operating characteristic curves for the classifications, complete - partial - insensitive. Three curves are displayed considering one class versus the others with and without the use of the residual fields (respectively plain and dashed curves). When considering the LE and REC only, the AUC of the complete -

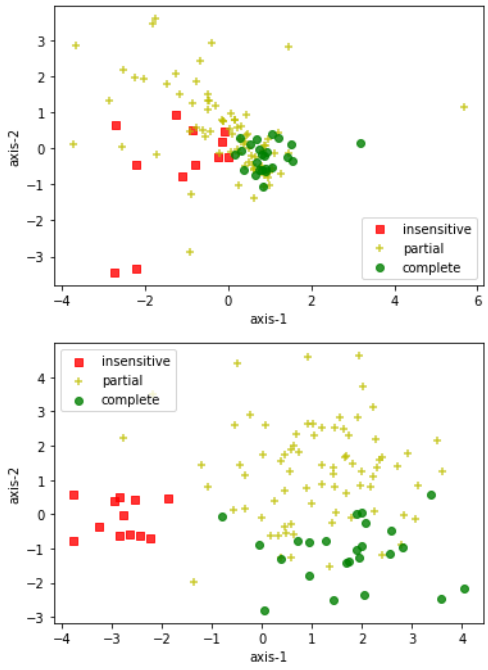

Fig. 3. Lesion features projected onto the first LDA components. (top) using only LE and REC features and (bottom) considering the residual features.

partial - insensitive responses are 0.86, 0.66 and 0.84. When considering the LE, REC and residual features, the AUC of the complete - partial - insensitive responses are 0.94, 0.86 and 0.98.

5. DISCUSSION

When registered, the blue and red pattern, initially being the signature of an nonalignment, are now related to density changes in the low-energy residuals and iodine uptake change in the recombined residuals. It is to be noted that the registration of projections is also polluted by the signature of 3D projected motion that cannot be corrected by in-plane displacements (*e.g.,* vertical shear). Hence, part of the final residual comes from this uncorrected 3D motions.

In general, it can be seen that the low-energy residual gives a piece of new information on the lesion evolution. It is well correlated with the iodine residual and with the lesion annotation performed by the radiologist. Lesion intensity evolution that may be difficult to read in the LE images can be more easily identified when registered. For a more details on the registration procedure and registration parameter selection, the reader can refer to [19].

The classification results were obtained using the GDIC-I registration approach as many cases did not converge with the other registration techniques. GDIC-I significantly outperformed the other approaches on all registration metrics. The classification model performed better, on all metrics: AUC and F-score, when taking into account the residual features. Instead of considering only the evolution of global features (*e.g.,* delta radiomics approaches[20]), the registered approach allows considering features of the evolution. As those residuals highlight the pixel-wise intensity changes, they are clear piece of information monitoring the lesion evolution.

The visual evaluation of the two first LDA components showed a better separation between the three clusters. Finally, the ROC curves

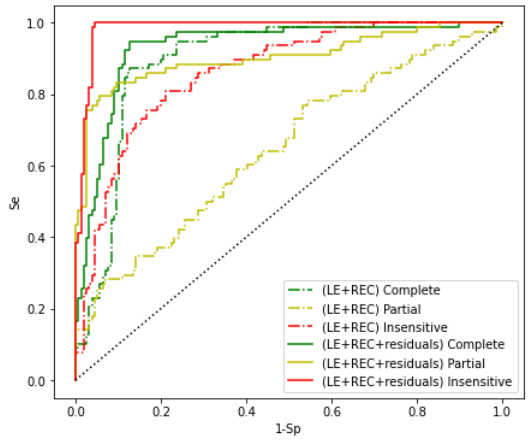

Fig. 4. ROC curves for the classification considering one class versus the others. Dashed curves are obtained with LE and REC features. Plain curves are obtained with LE, REC and residual features.

showed a better classification for all three classes when taking into account the registered features. The two extreme responses (complete and insensitive) had the best classification results. As the three classes can be seen with a continuous evolution on a clinical scale, with the partial response being the intermediate class, it is expected that this last class has the weakest results.

The limitation of this study is the small number of NAC-CEM cases (containing only 6 insensitive cases). An extension of this work with additional cases will allow including more radiomic features and more efficient classification models.

6. CONCLUSION

A robust non-rigid registration method, GDIC-I, handling large motion, important intensity changes and showing a high convergence rate has been proposed. The approach consists of identifying smooth kinematics and an intensity field compensating for local texture changes.

The proposed registration approach was compared to the standard state-of-the-art registration techniques. Those classical methods are very sensitive to large breast texture changes and fail when registering NAC cases with large lesion evolution. Different metrics were used and better results were obtained with the proposed approach.

The registration benefit was demonstrated by using a tumor response classification model that gave better classification results (AUC and F1 score) when considering residual fields features. One limit of this work lies in the small CEM-NAC dataset. An extension of this work with additional data could consist in a larger radiomics extraction and a more complex, non-linear model. With additional data, the classification of the shrinkage pattern could also be enhanced with the residual fields features. In addition, instead of performing independent predictions, the classification model could leverage both CC and MLO views.

Finally, the precise assessment of the tumor response is a key clinical feature for the radiologist, the surgeon and the oncologist. The AI assessment could be included in the discussion for the management of the patient care pathway.

7. ACKNOWLEDGMENTS

The authors would like to acknowledge Asmaa Alaa (*Baheya Foundation For Early Detection And Treatment Of Breast Cancer*), Razvan Iordache (*GE HealthCare*), and Jean-Paul Antonini (*GE HealthCare*) for their help in the data collection.

8. COMPLIANCE WITH ETHICAL STANDARDS

This research study was conducted retrospectively using anonymized human subject data made available by *Baheya Foundation For Early Detection And Treatment Of Breast Cancer, Giza, Egypt*. Applicable law and standards of ethic have been respected.

9. REFERENCES

[1] Y. Ou, S.P. Weinstein, E.F. Conant, S. Englander, X. Da, B. Gaonkar, M.-K. Hsieh, M. Rosen, A. DeMichele, C. Davatzikos, et al., "Deformable registration for quantifying longitudinal tumor changes during neoadjuvant chemotherapy," *Magnetic resonance in medicine*, vol. 73, no. 6, pp. 2343–2356, 2015.

[2] S. Riyahi, W. Choi, C.-J. Liu, H. Zhong, A.J. Wu, J.G. Mechalakos, and W. Lu, "Quantifying local tumor morphological changes with jacobian map for prediction of pathologic tumor response to chemo-radiotherapy in locally advanced esophageal cancer," *Physics in Medicine & Biology*, vol. 63, no. 14, pp. 145020, 2018.

[3] C. Dromain, F. Thibault, S. Muller, F. Rimareix, S. Delaloge, A. Tardivon, and C. Balleyguier, "Dual-energy contrast-enhanced digital mammography: initial clinical results," *European radiology*, vol. 21, no. 3, pp. 565–574, 2011.

[4] V. Iotti, S. Ravaioli, R. Vacondio, C. Coriani, S. Caffarri, R. Sghedoni, A. Nitrosi, M. Ragazzi, E. Gasparini, C. Masini, et al., "Contrast-enhanced spectral mammography in neoadjuvant chemotherapy monitoring: a comparison with breast magnetic resonance imaging," *Breast Cancer Research*, vol. 19, no. 1, pp. 1–13, 2017.

[5] B.K. Patel, T. Hilal, M. Covington, N. Zhang, H.E. Kosiorek, M. Lobbes, D.W. Northfelt, and B.A. Pockaj, "Contrast-enhanced spectral mammography is comparable to MRI in the assessment of residual breast cancer following neoadjuvant systemic therapy," *Annals of surgical oncology*, vol. 25, no. 5, pp. 1350–1356, 2018.

[6] R.M. Kamal, S.M. Saad, A.F.I. Moustafa, M.M. Gomaa, O. Mokhtar, I. Gouda, A. Hassan, A. Hilal, and A. ElZayat, "Predicting response to neo-adjuvant chemotherapy and assessment of residual disease in breast cancer using contrast-enhanced spectral mammography: a combined qualitative and quantitative approach," *Egyptian Journal of Radiology and Nuclear Medicine*, vol. 51, no. 1, pp. 1–14, 2020.

[7] D. Xing, N. Mao, J. Dong, H. Ma, Q. Chen, and Y. Lv, "Quantitative analysis of contrast enhanced spectral mammography grey value for early prediction of pathological response of breast cancer to neoadjuvant chemotherapy," *Scientific Reports*, vol. 11, no. 1, pp. 1–9, 2021.

[8] Z. Wang, F. Lin, H. Ma, Y. Shi, J. Dong, P. Yang, K. Zhang, N. Guo, R. Zhang, J. Cui, et al., "Contrast-enhanced spectral mammography-based radiomics nomogram for the prediction of neoadjuvant chemotherapy-insensitive breast cancers," *Frontiers in Oncology*, vol. 11, pp. 84, 2021.

[9] Y. Li, H. Chen, Y. Yang, L. Cheng, and L. Cao, "A bilateral analysis scheme for false positive reduction in mammogram mass detection," *Computers in biology and medicine*, vol. 57, pp. 84–95, 2015.

[10] Y. Díez, A. Oliver, X. Llado, J. Freixenet, J. Marti, J.C. Vilanova, and R.t Marti, "Revisiting intensity-based image registration applied to mammography," *IEEE Transactions on Information Technology in Biomedicine*, vol. 15, no. 5, pp. 716–725, 2011.

[11] L. Zhang, Y. Li, H. Chen, and L. Cheng, "Mammographic mass detection by bilateral analysis based on convolution neural network," in *2019 IEEE International Conference on Image Processing (ICIP)*. IEEE, 2019, pp. 784–788.

[12] C. Zach, T. Pock, and H. Bischof, "A duality based approach for realtime TV-L1 optical flow," in *Joint pattern recognition symposium*. Springer, 2007, pp. 214–223.

[13] G. Besnard, F. Hild, and S. Roux, ""Finite-element" displacement fields analysis from digital images: application to Portevin–le Châtelier bands," *Experimental Mechanics*, vol. 46, no. 6, pp. 789–803, 2006.

[14] A. Mendoza, J. Schneider, E. Parra, and S. Roux, "The correlation framework: Bridging the gap between modeling and analysis for 3d woven composites," *Composite Structures*, vol. 229, pp. 111468, 2019.

[15] M. Holden, "A review of geometric transformations for nonrigid body registration," *IEEE transactions on medical imaging*, vol. 27, no. 1, pp. 111–128, 2007.

[16] J. Réthoré, S. Roux, and F. Hild, "An extended and integrated digital image correlation technique applied to the analysis of fractured samples: The equilibrium gap method as a mechanical filter," *European Journal of Computational Mechanics/Revue Européenne de Mécanique Numérique*, vol. 18, no. 3-4, pp. 285–306, 2009.

[17] C. Jailin, P. Milioni, Z. Li, R. Iordache, and S. Muller, "Lesion detection in contrast enhanced spectral mammography," in *16th International Workshop on Breast Imaging (IWBI2022)*. SPIE, 2022, vol. 12286, pp. 54–61.

[18] T. Fawcett, "An introduction to roc analysis," *Pattern recognition letters*, vol. 27, no. 8, pp. 861–874, 2006.

[19] C. Jailin, P. Milioni, S. Mohamed, L. Vancamberg, A. Farouk, M.M. Gomaa, R.M. Kamal, and S. Muller, "Deformable registration with intensity correction for CEM Neoadjuvant Chemotherapy," *Biomedical Physics & Engineering Express*, 2023.

[20] V. Nardone, A. Reginelli, R. Grassi, L. Boldrini, G. Vacca, E. D'Ippolito, S. Annunziata, A. Farchione, M.P. Belfiore, I. Desideri, and S. Cappabianca, "Delta radiomics: A systematic review," *La radiologia medica*, vol. 126, no. 12, pp. 1571–1583, 2021.